Kang *et al. Biochar* (2023) 5:56
https://doi.org/10.1007/s42773-023-00250-w

Biochar

ORIGINAL RESEARCH

Open Access

Synthesis of Mg–K-biochar bimetallic catalyst and its evaluation of glucose isomerization

Xiheng Kang[1], Zi You[1], Jian Peng[1], Arthur J. Ragauskas[2,3,4*], Jingdong Pang[6], Peitao Zhao[5], Yongjun Yin[1] and Xueping Song[1*]

Abstract

Highly efficient isomerization of glucose to fructose is essential for valorizing cellulose fraction of biomass to value-added chemicals. This work provided an innovative method for preparing Mg-biochar and Mg–K-biochar catalysts by impregnating either $MgCl_2$ alone or in combination with different K compounds (Ding et al. in Bioresour Technol 341:125835, 2021, https://doi.org/10.1016/j.biortech.2021.125835 and $KHCO_3$) on cellulose-derived biochar, followed by hydrothermal carbonization and pyrolysis. Single active substance MgO existing in the $_{10}$Mg–C could give better catalytic effect on glucose isomerization than the synergy of MgO and KCl crystalline material present in $_{10}$Mg–KCl–C. But the catalytic effect of $_{10}$Mg–C was decreased when the basic site of MgO was overloaded. Compared to other carbon-based metal catalysts, $_{10}$Mg–$KHCO_3$–C with 10 wt% $MgCl_2$ loading had excellent catalytic performance, which gave a higher fructose yield (36.7%) and selectivity (74.54%), and catalyzed excellent glucose conversion (53.99%) at 100 °C in 30 min. Scanning electron microscope–energy dispersive spectrometer and X-Ray diffraction revealed that the distribution of Mg^{2+} and K^+ in $_{10}$Mg–$KHCO_3$–C was uniform and the catalytic active substances (MgO, KCl and K_2CO_3) were more than $_{10}$Mg–C (only MgO). The synergy effects of MgO and K_2CO_3 active sites enhanced the pH of reaction system and induced H_2O ionization to form considerable OH^- ions, thus easily realizing a deprotonation of glucose and effectively catalyzing the isomerization of glucose. In this study, we developed a highly efficient Mg–K-biochar bimetallic catalyst for glucose isomerization and provided an efficient method for cellulose valorization.

Highlights

(a) The bimetallic Brønsted catalyst designed in this study ($_{10}$Mg–$KHCO_3$–C) could achieve high fructose yield (36.7%) and selectivity (74.54%).
(b) The MgO could give obtain good catalytic effect on glucose isomerization, but the catalytic effect decreased when the Mg^+ was overloaded.

Handling editor: Bin Gao.

*Correspondence:
Arthur J. Ragauskas
aragausk@utk.edu
Xueping Song
sx_ping@gxu.edu.cn
Full list of author information is available at the end of the article

Springer

© The Author(s) 2023. **Open Access** This article is licensed under a Creative Commons Attribution 4.0 International License, which permits use, sharing, adaptation, distribution and reproduction in any medium or format, as long as you give appropriate credit to the original author(s) and the source, provide a link to the Creative Commons licence, and indicate if changes were made. The images or other third party material in this article are included in the article's Creative Commons licence, unless indicated otherwise in a credit line to the material. If material is not included in the article's Creative Commons licence and your intended use is not permitted by statutory regulation or exceeds the permitted use, you will need to obtain permission directly from the copyright holder. To view a copy of this licence, visit http://creativecommons.org/licenses/by/4.0/.

(c) The synergy effects of MgO and K_2CO_3 could enhance the pH of reaction system and effectively catalyze the isomerization of glucose.

Keywords Isomerization, Catalyst, Fructose, Biochar, MgO

Graphical Abstract

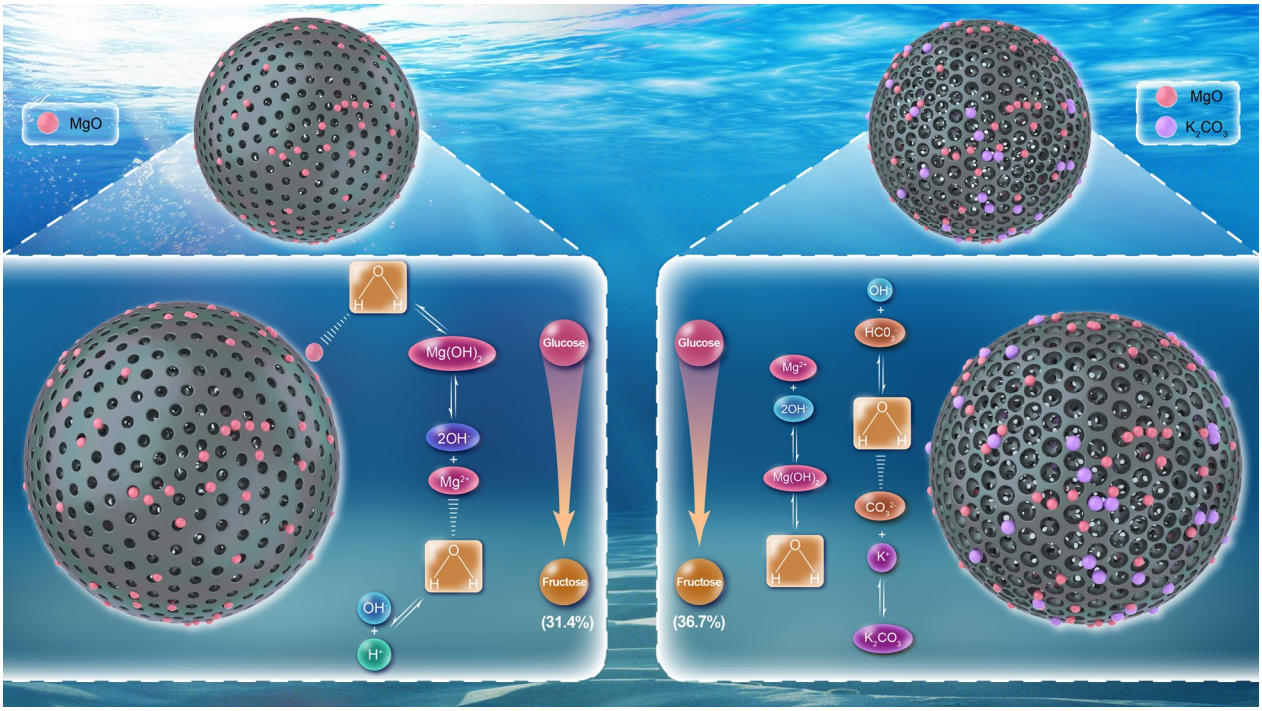

1 Introduction

The current high global population has increased the consumption of chemicals considerably, and the catalytic conversion of biomass feedstocks into renewable chemicals has attracted a lot of attention. Cellulose is a polymer composed of several glucose monomers linked through β-1,4-glycosidic bonds. It is also the most abundant component of lignocellulosic biomass (Kang et al. 2021). Fructose, structurally similar to glucose, is chemically more active than glucose and is easily converted to different molecules such as 5-hydroxymethylfurfural (5-HMF), furfural, and levulinic acid (LA). So, it is one of the most significant precursors for numerous chemicals. Presently, enzymatic glucose isomerization is the main method for efficient fructose preparation. However, glucose isomerase has some disadvantages, including low stability, poor accessibility, and harsh reaction conditions, and thus it is important and urgent to develop more efficient alternative catalysts.

Biochar is a solid product with a carbon skeleton and rich in oxygen-containing functional groups. It also has a large specific surface area and a tunable pore structure and thus has been widely used in high-quality carbon-based carriers (Deng et al. 2020; Falco et al. 2011; Kim et al. 2020). Carbon-based catalysts can mediate efficient isomerization (Kuichuan Sheng et al. 2019; Yang et al. 2012; Yu et al. 2019; Zhang et al. 2020a). Iris Yu et al. successfully prepared carbon-based catalysts with high Brønsted basic sites for catalytic glucose isomerization, which could obtain 12.8 mol% fructose yield in aqueous solution at 160 °C for 5 min (Yu et al. 2019). Additionally, Fu et al. fabricated a mesoporous carbon catalyst with high Brønsted basic sites, which could obtain 32.4% fructose yield with a selectivity up to 81.1%, in the glucose isomerization process (Fu et al. 2021a). However,

compared to inorganic materials-based carriers, the weak interaction forces between the carbon-based carriers and the active sites make the carbon-base carriers unable to achieve high stability. The low-cost controlled physical and chemical properties make them comparable to carrier catalysts based on inorganic materials in terms of catalytic efficiency. In terms of physical properties, the catalytic efficiency of carbon-based catalysts usually can be enhanced by modifying the porosity, specific surface area, and crystalline structure of biochar (Fu et al. 2021b). Recent studies have shown that the catalytic efficiency of glucose isomerization enhanced by the chemical loading of metal-active substances is more than by optimizing the physical properties of biochar. Brønsted basic-site catalysts provided by the basic metal oxides in hydrotalcite also significantly contribute to glucose isomerization (Liu et al. 2021c). Compared with the effects of different catalysts (ZSM-5, γ-Al_2O_3, SiO_2/Al_2O_3, TiO_2, ZrO_2/TiO_2, MgO) on the isomerization of glucose, it has been revealed that higher Brønsted basic sites are effective in achieving higher fructose selectivity (Marianou et al. 2016). MgO is a highly alkaline substance, and it can be hydrolyzed in aqueous to form OH^- ions. Its log K_b value is 21.36 (Zhang et al. 2020b). Marianou et al. prepared MgO catalysts and the optimum catalyst could reach 44.1 wt% glucose conversion and 75.8 wt% fructose selectivity (33.4 wt% fructose yield) at 90 °C for 45 min reaction in aqueous solution (Marianou et al. 2018). In addition, methods of impregnating Mg into other materials have also been studied. Dr. Rabee et al. further explored MgO impregnated ZrO_2 with different Mg/Zr atomic ratios to prepare the catalyst for glucose isomerization process (Rabee et al. 2020). The results showed that MgO–ZrO_2 could obtain fructose yield of 33% at 95 °C after 3 h. The catalytic effect of alkaline Brønsted catalysts is obtained through OH^- ions to promote the deprotonation of glucose to form an enediol intermediate, which is mainly related to the catalytic pathway of Brønsted catalysts (Marianou et al. 2016; Suttibut et al. 2015). However, the few unsaturated catalytic sites make Brønsted basic catalysis difficult to simultaneously ensure high glucose conversion and fructose selectivity. In addition, overexposed basic sites also attack the fructose to undergo a re-isomerization reaction, leading to a decrease in the yield of fructose. Therefore, how to tailor the content and species of catalytic sites in the catalyst is a key to improving the efficiency of Brønsted catalysts.

In the study, in order to enhance glucose isomerization efficiency, Mg–K–C biochar-based bimetallic catalysts were prepared, which can provide more catalytic sites while altering the morphology of catalyst and increasing the contact area of the active sites. And the synergistic effects of both Mg^{2+} and K^+ metal compound catalysts on the conversion of glucose, the yield and selectivity of fructose were investigated. The active catalytic substances in the catalyst, their catalytic efficiency, and the catalytic mechanisms for glucose isomerization were further defined. This work will provide excellent technical support for developing biochar-based glucose isomerization catalysts and high-quality biomass platform products.

2 Materials and methods

2.1 Materials

The glucose, MgO, $MgCl_2$, KCl, KOH, $KHCO_3$, and K_2CO_3 used in this work were of analytical grade and were purchased from Aladding Co., Ltd. (Shanghai, China). Cellulose (particle size < 50 μm) was purchased from Aladding Co., Ltd. (Shanghai, China). All standard reagents (glucose, fructose) were supplied by Sigma-Aldrich of Merck KGaA Co., Ltd. (Germany) and were used without further purification. Milli-Q® ultrapure water purification system supplied ultrapure water (Merck KGaA, Germany).

2.2 Preparation of biochar

10 g of cellulose and 100 mL deionized water were mixed in a 500 mL autoclave reactor (BS-500, Shanghai LABE Instrument Co., Ltd), and then heated from room temperature to 220 °C and kept for 240 min. After the reaction, the reactor was cooled rapidly with ice-cold water to stop the reaction. All the biochar and liquid phase products in the reactor were collected, and the biochar was separated by centrifuging at 10,000 rpm for 8 min. The biochar product was washed repeatedly with ultrapure water and ethanol to a pH of 7.0. The biochar, denoted as C, was obtained after drying to a constant weight at 80 °C.

2.3 Synthesis of Mg–C catalyst

Mg-supported biochar catalysts were prepared through an impregnation-carbonization method. Firstly, in the aqueous solution, 1 g of C was mixed with different masses of $MgCl_2$ (5 wt%, 10 wt%, and 20 wt% of C). Then, these mixtures were stirred for 4 h and dried at 80 °C to a constant weight, respectively. The dried mixture was pyrolyzed in a tube furnace in a N_2 atmosphere (the flow rate is 1.5 L min^{-1}) at a ramp rate of 10 °C min^{-1} from room temperature to 650 °C and kept for 60 min (Ahmad et al. 2016, 2020). At the end of the reaction, all the Mg–C catalysts were removed and placed in a desiccator. All the Mg–C catalysts after pyrolyzed were used immediately after preparation to avoid deactivation in air. The obtained Mg–C catalysts with initial Mg loading of 0 wt%, 5 wt%, 10 wt%, and 20 wt% were denoted as $_5$Mg–C,

$_{10}$Mg–C, and $_{20}$Mg–C, respectively. The control sample ($_{0}$Mg–C) without the $MgCl_2$ was prepared according to above conditions.

2.4 Synthesis of Mg–K–C catalyst

1 g of KCl, KOH, $KHCO_3$, and K_2CO_3 were dissolved separately in deionized water (60 mL), and then mixed with the $_{10}$Mg–C. The mixture was stirred with a magnetic stirrer for 4 h, and then dried at 80 °C for 12 h. The dried mixture was pyrolyzed in a tube furnace in N_2 atmosphere (the flow rate is 1.5 L min^{-1}) at a ramp rate of 10 °C min^{-1} from room temperature to 650 °C and maintained at this temperature for 60 min. At the end of the reaction, all the Mg–K–C catalysts were removed and placed in a desiccator. All the Mg–K–C catalysts after pyrolyzed were used immediately after preparation to avoid deactivation in air. The $_{10}$Mg–K–C catalysts with KCl, KOH, $KHCO_3$, and K_2CO_3 activators were denoted as $_{10}$Mg–KCl–C, $_{10}$Mg–KOH–C, $_{10}$Mg–$KHCO_3$–C, and $_{10}$Mg–K_2CO_3–C, respectively.

2.5 Catalytic experiment

Glucose (10% wt/v) was added to a water suspension containing 0.1 g of C or Mg–C or $_{10}$Mg–K–C, respectively. The control catalyst was C and MgO. In the Mg–C catalytic experiment, the mixture of glucose and Mg–C was placed in an autoclave reactor (500 mL), heated to target temperatures (80, 100, 120, and 140 °C), and maintained at the target temperature for different times (10, 20, 30, and 40 min). In the C and MgO catalytic experiment, the mass of C and MgO was determined according to the Mg element and accounted for 10 wt% of C, and the mixture of glucose and C or MgO was placed in an autoclave reactor (500 mL) and heated to 100 °C, maintained at 100 °C for 30 min. Likewise, in the Mg–K–C catalytic experiment, the mixture of glucose and Mg–K–C was placed in an autoclave reactor (500 mL) and heated to 100 °C, and then maintained for 30 min. During the catalytic experiment, the mixtures were magnetically stirred at 300 r min^{-1} to maintain homogeneity. At the end of the catalytic experiment, the residual catalyst of $_{10}$Mg–C and $_{10}$Mg–$KHCO_3$–C was washed with deionized (DI) water and then dried at 80 °C to a constant weight. The dried residual catalyst would be used to continually conduct repeated glucose post-isomerization experiments following the above experimental steps under the conditions of 100 °C for 30 min, to analyze the stability of catalyst. And the glucose solution after repeated post-isomerization experiment was used for the detection of Mg leaching. The number of times the catalyst was used repeatedly was denoted as X. For example, $_{10}$Mg–$KHCO_3$–C-3 means that $_{10}$Mg–$KHCO_3$–C was used three times. All experiments were performed in triplicate. The results represent an average of three experiments and a standard deviation of 1.5%.

2.6 Characterization of biochar

Brunauer–Emmett–Teller (BET) surface areas and pore volumes were determined using N_2 adsorption–desorption isotherm measurements at−196 °C using a gas sorption analyzer (Micro Meritics; ASAP 2460). The samples were degassed at 80 °C for 16 h before analysis. The samples' surface morphology and elemental composition were evaluated using scanning electron microscopy (SEM) coupled with energy-dispersive X-ray spectroscopy (TESCAN MIRA4). The crystalline and amorphous phases were evaluated using X-ray direction analysis (XRD; MiniFlex 600) at a scanning range of 10–90° at a rate of 5° min^{-1} under 40 kV and 40 mA. The chemical state of elements on sample surfaces was evaluated using X-ray photoelectron spectroscopy (XPS; Thermo Fisher Scientific K-Alpha ESCA). Solid-state ^{13}C-NMR experiments were performed using a Bruker 400M spectrometer equipped with 4-mm zirconia rotors as sample holders and under a spinning MAS rate of 10 kHz. The chemical shift reference was tetramethylsilane (0 ppm). The metal quantitative analysis of the samples was evaluated using an inductively coupled plasma optical emission spectrometer (Agilent Technology; ICP-OES 700).

2.7 Characterization of catalytic efficiency

The concentrations of glucose and fructose in the liquid phase were quantified by HPLC (Agilent 1200 Series, Santa Clara, CA, USA) using a Bio-Rad HPX-87H column (300×7.8 mm). Sulfuric acid (5 mM, 0.6 mL min^{-1} flow rate) was used as the eluent, and the column temperature was maintained at 50 °C (Kang et al. 2022). Glucose and fructose concentrations were determined using calibration curves obtained with the reference samples. The conversion of glucose and the yield and selectivity of fructose were calculated as follows:

$$C_{Glu}(\%) = \frac{(I_{Glu} - R_{Glu})}{I_{Glu}} \times 100\%$$

$$S_{Fru}(\%) = \frac{I_{Fru}}{(I_{Glu} - R_{Glu})} \times 100\%$$

$$Y_{Fru}(\%) = \frac{I_{Fru}}{I_{Glu}} \times 100\%,$$

where I_{Glu} and R_{Glu} represent the initial and final moles of glucose, respectively. I_{Fru} represents the moles of fructose.

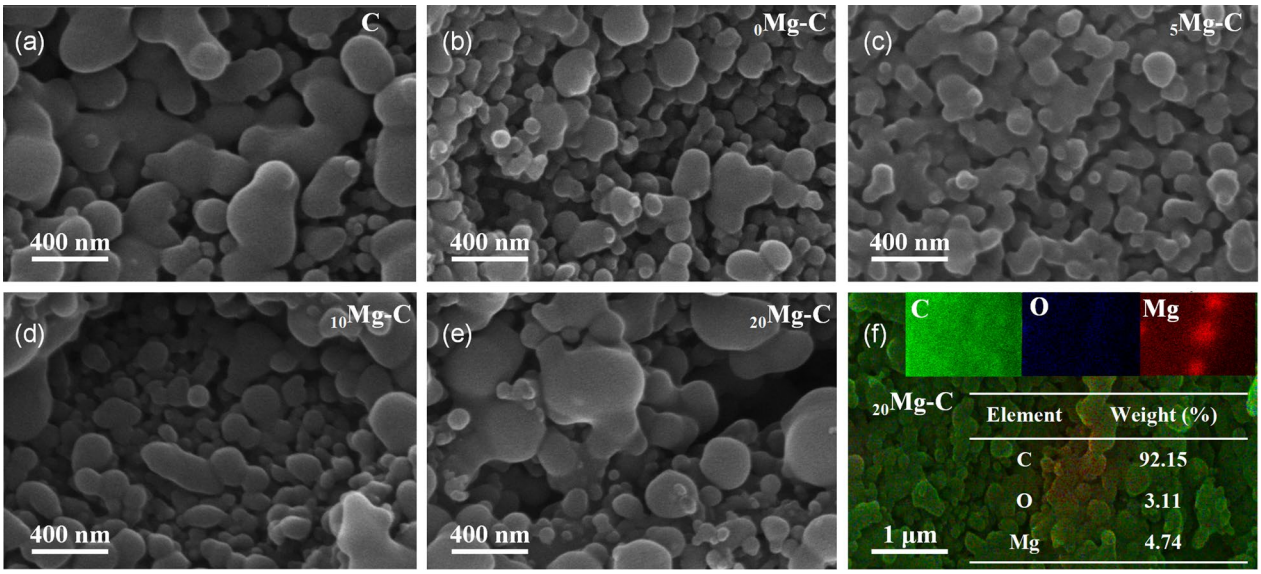

Fig. 1 SEM images of Mg–C catalysts with different Mg loadings: **a** C, **b** $_0$Mg–C, **c** $_5$Mg–C, **d** $_{10}$Mg–C, **e** $_{20}$Mg–C, and **f** EDS analysis of $_{20}$Mg–C

3 Results and discussion

3.1 Characterization of Mg–C catalyst

The results of loading capacity of Mg^{2+} ions in Mg–C showed that Mg^{2+} ions were successfully loaded into the biochar (Additional file 1: Fig. S1). As shown in Fig. 1f, the distribution of C and O elements on the surface of $_{20}$Mg–C was uniform, but there was a significant aggregation of Mg^{2+} ions on the surface of $_{20}$Mg–C. The scanning electron microscope–energy dispersive spectrometer (SEM–EDS) results showed that Mg^{2+} ions did not overlap with O elements on the surface of $_{20}$Mg–C. From the images of SEM–EDS, it is speculated that the Mg^{2+} ions should be adsorbed on the surface of the Mg–C catalyst and may create new chemical substance (MgO) (Kim et al. 2015; Lazzarini et al. 2016).

The N_2 adsorption and desorption curves and pore-size distribution of Mg–C catalysts with different Mg loading amounts are shown in Fig. 2. According to the International Union of Pure and Applied Chemistry (IUPAC) classification of adsorption curves, all the

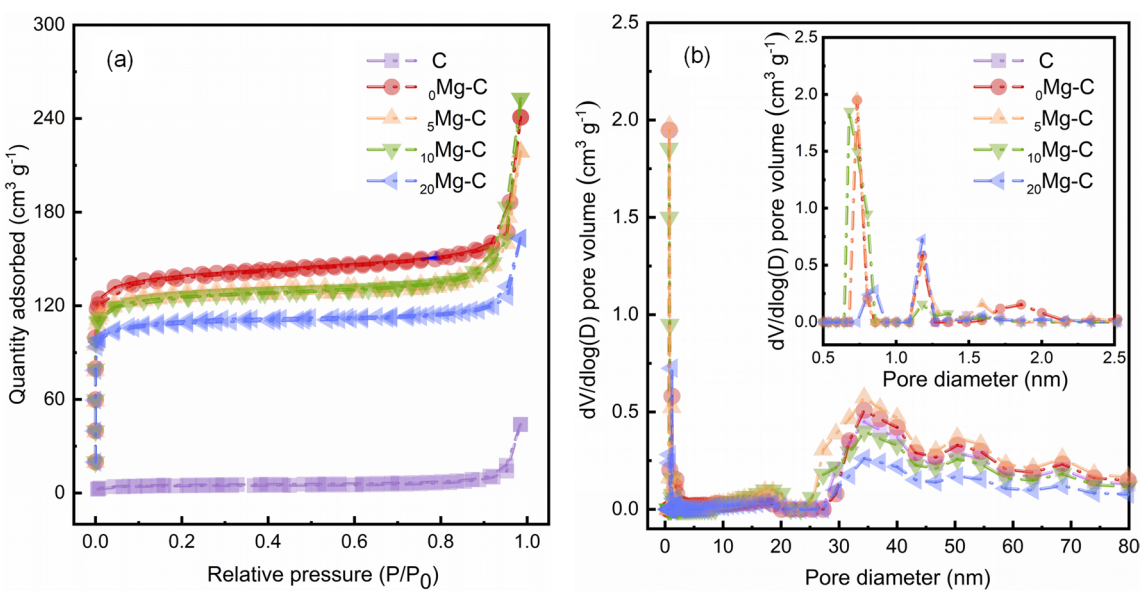

Fig. 2 Pore properties of Mg–C **a** N_2 adsorption and desorption isotherms, and **b** pore size distributions (inset)

Table 1 The BET surface area and pore size of Mg-C catalyst

Sample	S_{BET} (m^2 g^{-1})	S_{micro} (m^2 g^{-1})	S_{micro}/S_{BET} (%)	V_{micro} (cm^3 g^{-1})	Pore size (nm)
C	36.13	20.42	56.52	0.0089	1.03
$_0$Mg–C	460.77	385.08	83.57	0.1989	1.63
$_5$Mg–C	437.61	371.22	84.83	0.1807	1.60
$_{10}$Mg–C	416.16	360.71	86.68	0.1798	1.65
$_{20}$Mg–C	378.22	333.91	88.28	0.1591	1.61

adsorption and desorption isotherms of Mg–C show type I isotherm, demonstrating that the structure of Mg–C is predominantly microporous. The results of pore-size distribution diagram (Fig. 2b) showed that the pores in Mg–C were mainly micropores (0.5–1.5 nm) and a few mesopores (10–50 nm). Table 1 shows the specific surface area and pore properties parameters of Mg–C catalysts. Due to the high-temperature carbonization, the specific surface area and microporous volume of Mg–C catalysts decreased from 460.77 to 378.22 m^2 g^{-1} and from 0.1989 to 0.1591 cm^3 g^{-1} when the Mg loading amount was increased from 0 to 20 wt%, respectively. Yin et al. reported the similar results that the high temperature carbonization will improve the specific surface area from 1.90 to 202.75 m^2 g^{-1} (Yin et al. 2021). However, as the Mg loading amount was increased from 5 to 20 wt%, there was an insignificant change in the specific surface area of Mg–C. Similarly, the results of Li et al. pointed out that the changes in the loading amount of MgO/NaY cannot affect the specific surface area significantly. Thus, it is inferred that Mg loading amount cannot affect the specific surface area of the carbon-based substrate (Li et al. 2018).

At the same time, the introduced active material formed by adding $MgCl_2$ hampers the improvement of specific surface area. The XRD results of Mg–C and C showed that C and $_0$Mg–C had no Mg diffraction peaks within the 2-Theta of 10–90° (Fig. 3a). The $_5$Mg–C had relatively intensive diffraction peaks at 2-Theta of 36.9°, 42.9°, 62.3°, 74.7°, and 78.7°, attributed to the 111, 200, 220, 311, and 222 lattice planes of MgO crystals, respectively. The diffraction peak of MgO crystals in $_{10}$Mg–C and $_{20}$Mg–C remains constant, but the peak area was increased with an increase Mg loading, indicating that the increase in Mg loading does not affect the stability of MgO crystal. The XRD results from Yin et al. also illustrated that the MgO is the most important crystal phase (Yin et al. 2021). To further illustrate the primary bonding mode of Mg and C, solid-state ^{13}C-NMR analyses were performed on Mg–C (Fig. 3b). A comparison of the solid-state ^{13}C-NMR spectra of $_0$Mg–C and $_{10}$Mg–C revealed that these are some ester groups at δ = 63 ppm, carboxylic acid groups at δ = 187 ppm, and carbon-based substrate groups at δ = 128 ppm in both catalysts (Kang et al. 2022). Compared with $_0$Mg–C, the displacement of the carboxyl peak in $_{10}$Mg–C may be due to the reaction of Mg ions with C–OH in the carboxyl group to form C–O–Mg bond. Meanwhile, the structure of the Mg–C catalyst was affected by the Mg loading amount. The different species occurring on the Mg–C surface were identified in the XPS spectra (Table 2, Fig. 3c–e). In all the catalysts studied herein, three different carbon groups were observed from C 1*s* peak (Table 2): C–C/C=C (284.6 eV), C–OH/C–O–C (286.0 eV), and C=O (288.0 eV) (Chai et al. 2019). These groups such as C–OH/C–O–C/–C=O on the surface of Mg–C catalyst originate from the poly-furan, aromatic structure of the carbon substrate itself. Moreover, three different oxygen groups were observed from O 1*s* spectra (Table 2): Mg–O (529.8 eV), –O=C (531.6 eV), and C–OH /C–O–C (533.0 eV) (Chai et al. 2019). Since the OH^- ions on the surface of C can provide reaction sites for the Mg^{2+} ions and normally the Mg^{2+} ion can only be bonded with O^{2-}, the ratio of the peak area of Mg–O increased from 3.96% to 18.30%, while the C–OH/C–O–C groups gradually decreased with the increase of Mg loading amount. The ^{13}C-NMR and XPS results both illustrated that the Mg ions reacted with the C–OH from carboxyl group to form C–O–Mg. Additionally, two different Mg groups were observed from Mg 1*s* and Mg 2*p* (Table 2), and the results indicated that Mg on the catalyst surface was mainly present in the form of MgO and $Mg(OH)_2$ (Liu et al. 2021c).

3.2 Mg–C catalytic performance and stability analysis

The catalytic isomerization performance of C, MgO, and Mg–C with different Mg loading amounts is shown in Fig. 4. As shown in Fig. 4a, in the absence of any catalysis, the glucose conversion efficiency was only 3.62%. Similar, the C obtained by high temperature carbonization only caused the conversion of little glucose (2.21%). Compared with the C, the pure metal oxide MgO can provide appreciable glucose conversion rate, but poor selectivity and yield. This is because the relatively high hydrolytic capacity of MgO (log K_b = 21.36) can generate numerous OH^- ions after hydrolysis and likely provide a

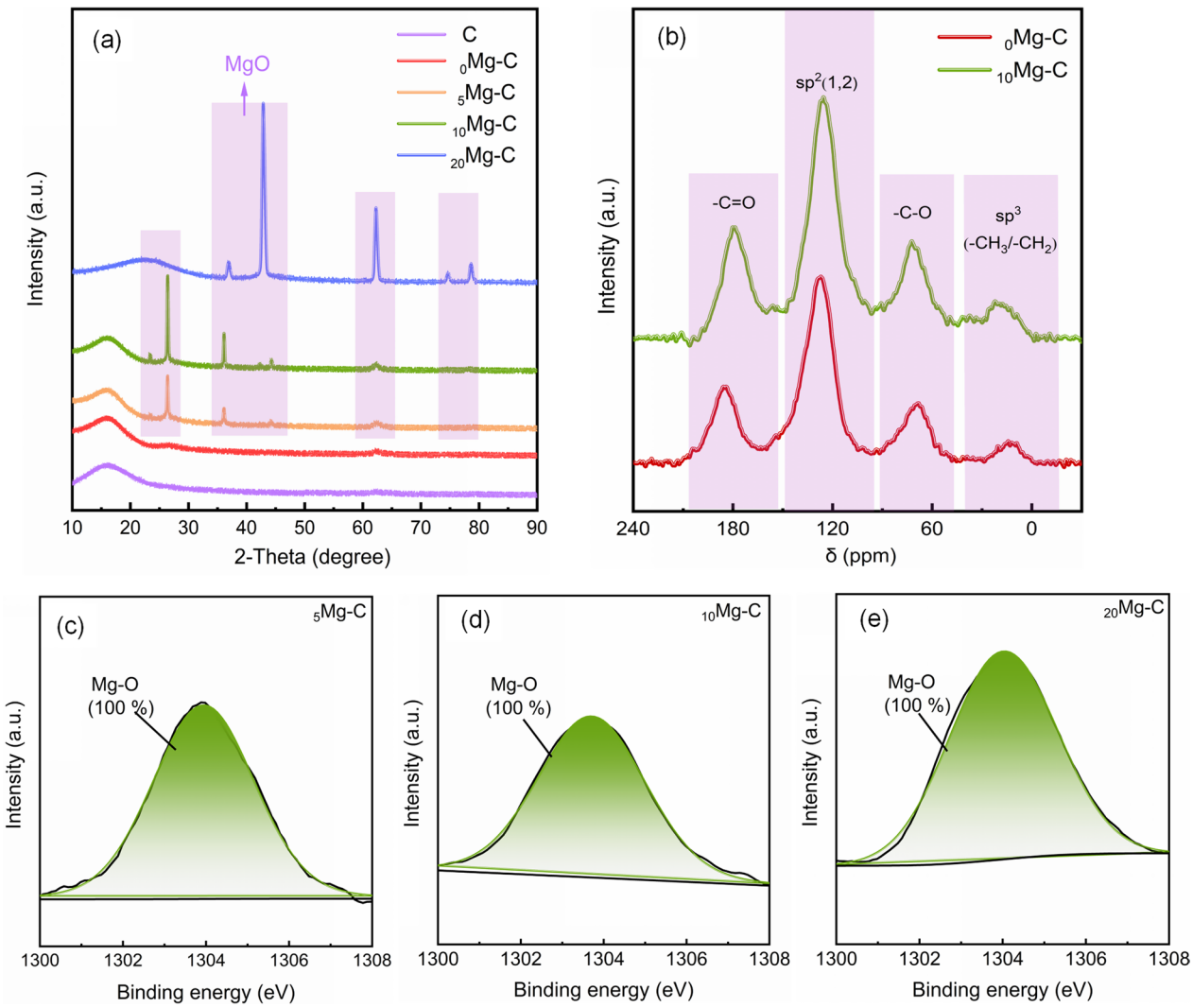

Fig. 3 Chemical properties of Mg–C **a** XRD, **b** solid-state ^{13}C-NMR spectra, and the XPS results of **c** $_5$Mg–C, **d** $_{10}$Mg–C, **e** $_{20}$Mg–C

Table 2 The XPS C 1s, O 1s, Mg 1s, and Mg 2p peak results of Mg–C

Sample	C 1*s*			O 1*s*			Mg 1*s*	Mg 2*p*	
	C–C/CHx/C=C (%)	C–OH/C–O–C (%)	–C=O (%)	C–OH/C–O–C (%)	–C=O (%)	Mg–O (%)	Mg–O (%)	Mg–O (%)	$Mg(OH)_2$ (%)
$_0$Mg–C	66.48	22.85	10.67	42.25	57.75	N.d.	N.d.	N.d.	N.d.
$_5$Mg–C	69.40	23.92	6.68	51.56	44.48	3.96	100.00	65.01	34.99
$_{10}$Mg–C	65.81	28.44	5.75	48.40	42.17	9.43	100.00	50.79	49.21
$_{20}$Mg–C	64.10	26.89	9.01	35.15	46.55	18.30	100.00	62.54	37.46

N.d. not detected

high catalysis conversion rate (Zhang et al. 2020b). So, the over-loading and the shedding of MgO on carbon-based carrier catalyst will affect the product distribution and catalytic efficiency. For this purpose, the catalytic efficiency of catalysts with different loading quantity of MgO was analyzed, and the results are shown in Fig. 4b. As the Mg loading quantity increased from 0 to 10 wt%, the glucose conversion peaked at 41.80%. The uniform distribution of active sites MgO on the surface of biochar can effectively improve the accessibility of active

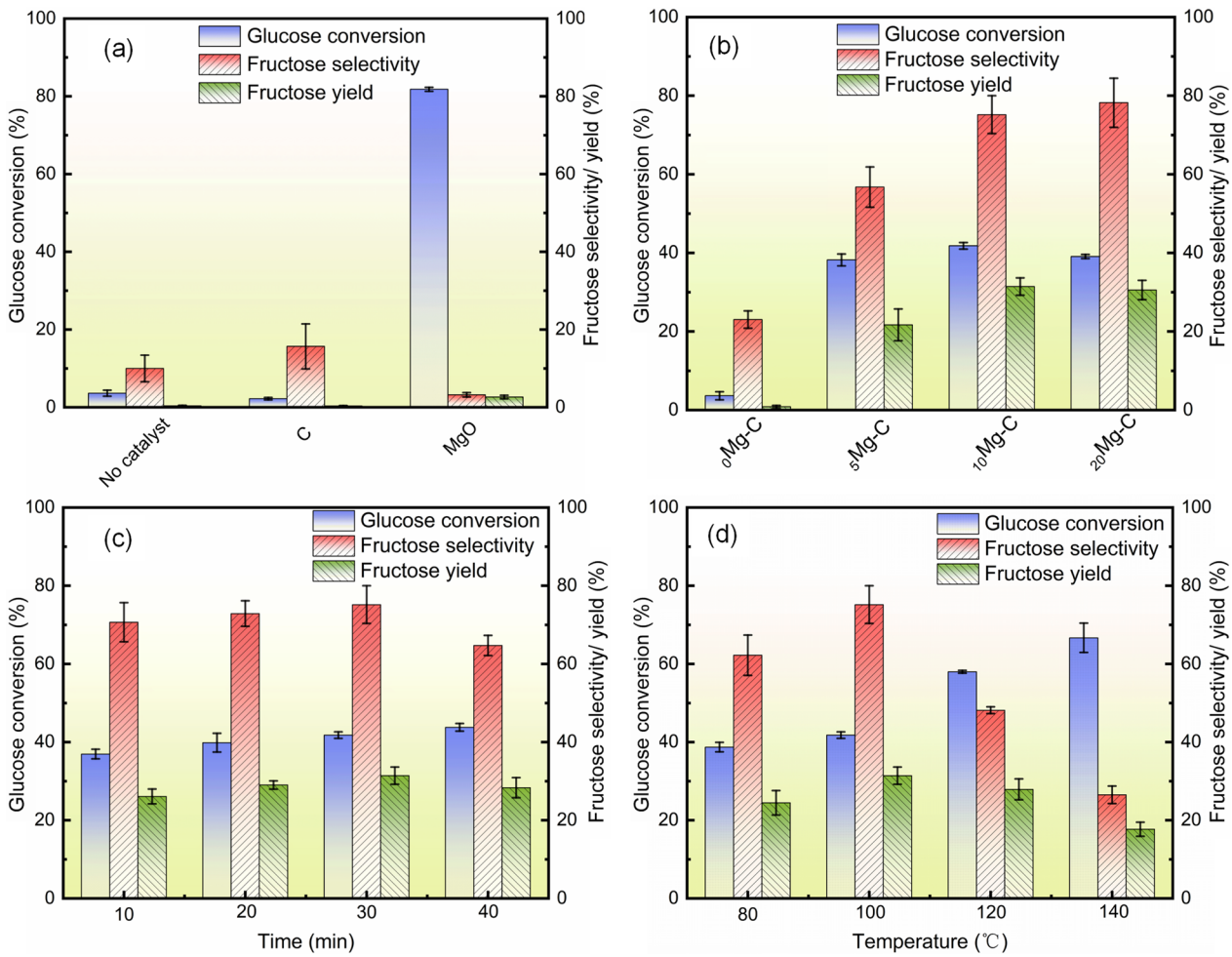

Fig. 4 Effects of **a** control, C, and MgO and **b** different Mg loading amount on the catalytic efficiency of glucose isomerization (conditions: 10 wt% glucose, 0.1 g catalyst, 100 °C, 30 min); effects of the different holding time (**c**), and temperatures (**d**) on the catalytic efficiency of glucose isomerization (conditions: 10 wt% glucose, 0.1 g $_{10}$Mg–C catalyst)

substances and glucose, preventing side reactions. When the Mg loading quantity increased from 10 to 20 wt%, the result of XRD (Fig. 3a) showed that both $_{10}$Mg–C and $_{20}$Mg–C had the diffraction peaks of MgO crystal. However, $_{20}$Mg–C had a higher peak intensity than $_{10}$Mg–C due to the overloading of Mg. Combined with the results of catalytic isomerization, these over-loaded basic sites attack the formed fructose to undergo a re-isomerization reaction, resulting in a decrease in the glucose conversion rate. Similar to the glucose conversion trend, the fructose selectivity as well as yields catalyzed by C and $_0$Mg–C were insignificant (Fig. 4a). The fructose yield and selectivity at 10 wt% loading reached 31.42% and 75.17%, respectively. The fructose yield at 20 wt% loading was similar to the 10 wt%, while the fructose selectivity decreased slightly. Therefore, the above results showed that an optimal Mg loading amount of 10 wt% yielded very high fructose from glucose. Figure 4c, d shows the catalytic efficiency of $_{10}$Mg–C at different temperatures and holding times. The effects of temperature on the catalytic efficiency were more significant than the holding time (Fig. 4c). The glucose conversion gradually increased from 38.73% to 41.80%, with an increase in temperature from 80 to 100 °C. The fructose yield and selectivity of 31.42% and 75.17% were achieved at 100 °C. As the temperature increased from 100 to 140 °C, the glucose conversion rate increased rapidly from 41.80% to 66.68%, whereas the fructose yield and selectivity increased rapidly to 17.73% and 26.54%, respectively.

The optimization of the holding time for the $_{10}$Mg–C catalyst was also performed. The results showed that glucose conversion increased from 36.95% to 41.80% when the holding time was extended from 10 to 30 min (Fig. 4d). The fructose yield and selectivity of 31.42% and 75.17% were achieved at holding time of 30 min. The glucose conversion rate increased to 43.78% as the

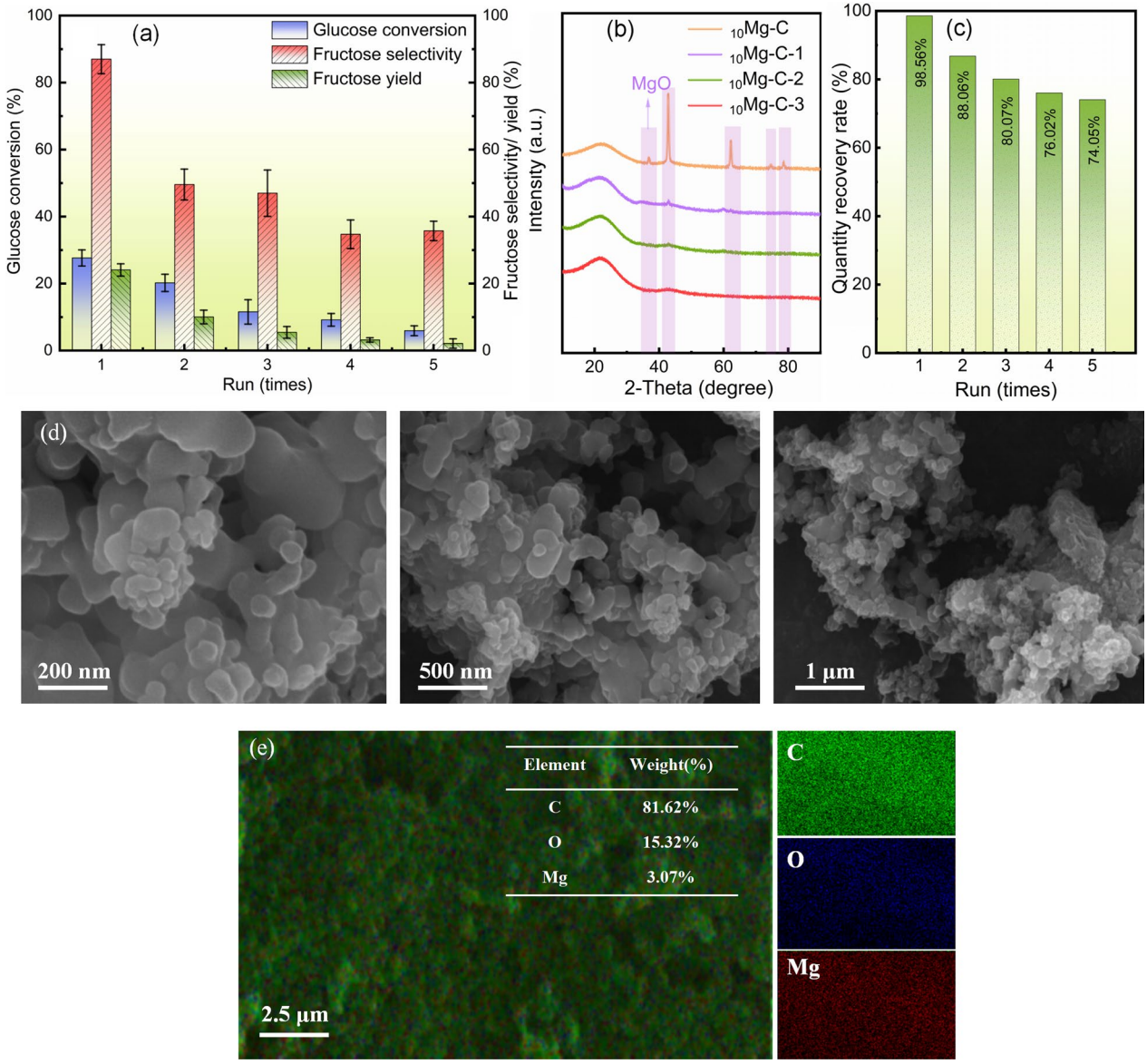

Fig. 5 Effects of $_{10}$Mg–C catalytic cycle times on **a** glucose isomerization catalytic efficiency, **b** XRD spectra, **c** recovery rate, and **d** SEM images and **e** SEM–EDS spectra

holding time was extended to 40 min, while the yield and selectivity of fructose decreased to 28.34% and 64.73%, respectively.

Notably, the effects of holding time on the glucose isomerization under $_{10}$Mg–C catalysis were not significantly different from that of temperature. Based on the above results, it can be concluded that the optimal Mg loading of the Mg–C catalyst is 10 wt%, and the optimal conditions for the catalytic process are 100 °C and 30 min, respectively. Moreover, the most critical factor affecting the catalytic efficiency is the catalyst type, followed by the reaction temperature, and the reaction time. This result is similar with the researches of Drabo consistent (Drabo et al. 2021).

The $_{10}$Mg–C catalyst was reused, and the recycled catalysts were further characterized to investigate its stability (Fig. 5). As shown in Fig. 5a, the glucose conversion and the fructose yield and selectivity deteriorated continuously with an increase in reuse times. The glucose conversion reduced from 41.80% to 29.86%, whereas the fructose yield and selectivitydecreased from 31.42% to 16.62%, and from 75.17% to 55.66%, respectively, after the first reuse. Meanwhile, the XRD (Fig. 5b) results indicated that the peak area of the MgO crystalline structure

significantly reduced. The MgO crystals almost completely disappeared after the third time use of the catalyst. At this moment, the glucose conversion and fructose yield decreased continually, whereas there was no significant changes in the fructose selectivity. The glucose conversion, fructose yield, and selectivity decreased rapidly to 4.38%, 0.36%, and 8.17% when the catalyst was used for the fourth time. After the catalyst was used four times, the SEM–EDS images of $_{10}$Mg–C demonstrated a loss of most of the crystal structure in $_{10}$Mg–C, and only 3.07% of Mg^{2+} ions were remained. The mass loss of recycled $_{10}$Mg–C is shown in Fig. 5(c). The mass loss of $_{10}$Mg–C gradually increased with an increase in the number of uses, peaking at 25.95% at the fifth use, consistent with SEM–EDS results.

Based on the above analysis, $_{10}$Mg–C catalysis achieved 75.17% fructose selectivity, yields 31.42% of fructose, and the conversion of 41.80% of glucose. However, the catalytic effect of $_{10}$Mg–C was inferior to that of glucose isomerase (Kuichuan Sheng et al. 2019). To further optimize the catalytic efficiency of the $_{10}$Mg–C catalyst, bimetallic $_{10}$Mg–K–C catalyst was prepared to enhance the alkaline catalytic site.

3.3 Characterization of Mg–K–C catalyst

SEM images of $_{10}$Mg–KCl–C, $_{10}$Mg–KOH–C, $_{10}$Mg–K_2CO_3–C, and $_{10}$Mg–$KHCO_3$–C, and SEM–EDS of $_{10}$Mg–$KHCO_3$–C are shown Fig. 6. As shown in the Fig. 6a–d, some crystals with uniform size and regular geometry were obtained after impregnation and carbonization with KCl and $KHCO_3$. The formation of uniformly sized crystals in the $_{10}$Mg–$KHCO_3$–C catalyst is mainly due to the reaction of $KHCO_3$ with $MgCl_2$ to produce crystalline active compounds such as MgO, KCl, and K_2CO_3 that encapsulate the carbon microspheres. The elemental surface distribution of Mg^{2+} and K^+ in $_{10}$Mg–$KHCO_3$–C was uniform based on the results of SEM–EDS. Compared to $_{10}$Mg–C, the distribution of Mg^{2+} ions and O^{2-} ions on the surface of $_{10}$Mg–$KHCO_3$–C overlapped. Meanwhile, the K element in the $_{10}$Mg–$KHCO_3$–C catalyst accounted for 19.99% of total element.

The nitrogen adsorption and desorption curves and the pores size distribution of different $_{10}$Mg–K–C catalysts are present in Fig. 7a, b. The BET surface area and pore size of $_{10}$Mg–K–C are shown in Table 3. The $_{10}$Mg–KCl–C catalyst was a type I isotherm, implying that $_{10}$Mg–KCl–C catalyst was mainly microporous. The $_{10}$Mg–KOH–C, $_{10}$Mg–K_2CO_3–C, and $_{10}$Mg–$KHCO_3$–C were type III isotherm, indicating the absence of significant pores. The pore size distribution diagram and BET surface area of catalysts also demonstrated the absence of significant pores in $_{10}$Mg–KOH–C, $_{10}$Mg–K_2CO_3–C, and $_{10}$Mg–$KHCO_3$–C. Combined with the results of SEM (Fig. 6) and XRD (Fig. 7c), some crystal substances of MgO and some amorphous structures of $MgCO_3$ on the biochar surface were found, which covered some pores thus resulting in low surface area (Table 3). Song et al. pointed out the similar conclusion that as the addition ratio of $KMnO_4$ to biochar increased from 2.5% to 10%, the biochar surface area decreased from 23.8 to 3.18 $m^2\ g^{-1}$ (Song et al. 2014).

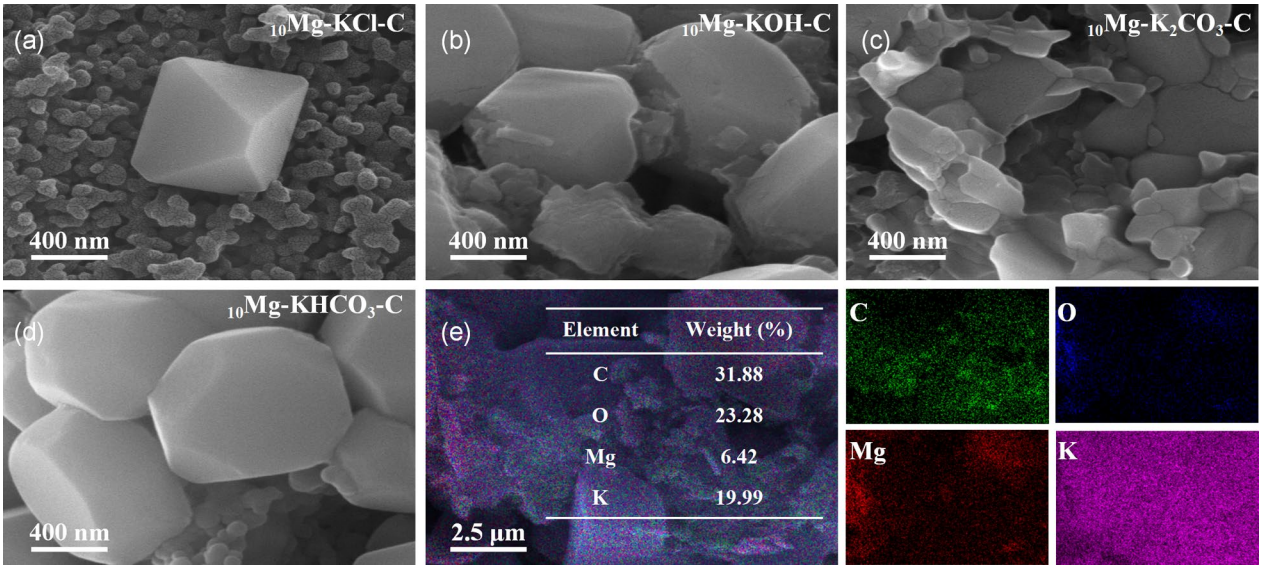

Fig. 6 SEM images of Mg–C catalysts with different Mg loadings: **a** $_{10}$Mg–KCl–C, **b** $_{10}$Mg–KOH–C, **c** $_{10}$Mg–K_2CO_3–C, **d** $_{10}$Mg–$KHCO_3$–C, and **e** EDS analysis of $_{10}$Mg–$KHCO_3$–C

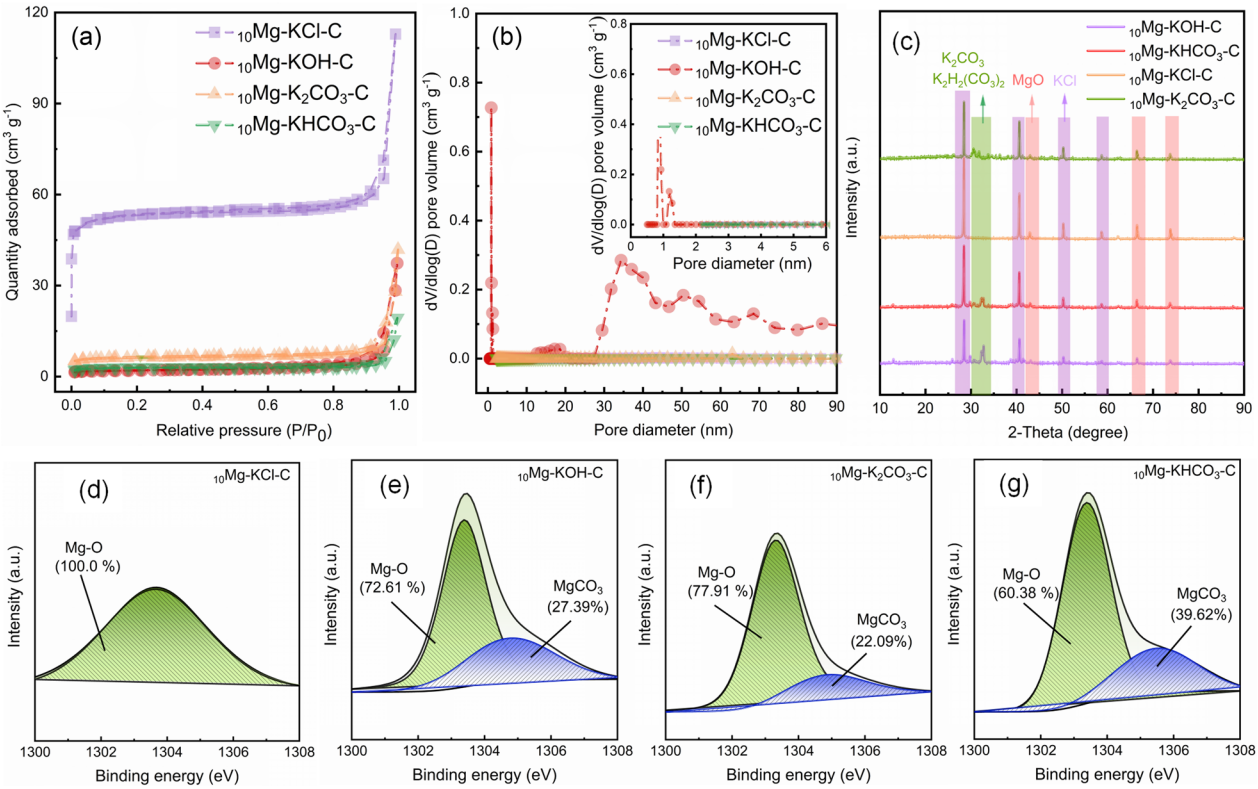

Fig. 7 Pore properties and XRD and XPS results of $_{10}$Mg–K–C **a** N_2 adsorption and desorption isotherms, **b** pore size distributions (inset) and **c** XRD spectra; XPS spectra of **d** $_{10}$Mg–KCl–C, **e** $_{10}$Mg–KOH–C, **f** $_{10}$Mg–K_2CO_3–C, and **g** $_{10}$Mg–$KHCO_3$–C

Table 3 The BET surface area and pore size of $_{10}$Mg–K–C catalyst

Sample	S_{BET} (m^2 g^{-1})	S_{micro} (m^2 g^{-1})	S_{micro}/S_{BET} (%)	V_{micro} (cm^3 g^{-1})	Pore size (nm)
$_{10}$Mg–C	416.16	360.71	86.68	0.1798	1.65
$_{10}$Mg–KCl–C	184.61	162.61	80.10	0.0726	1.61
$_{10}$Mg–KOH–C	6.60	3.43	51.97	0.0018	35.06
$_{10}$Mg–K_2CO_3–C	9.56	7.68	80.33	0.0038	12.50
$_{10}$Mg–$KHCO_3$–C	18.71	14.76	78.89	0.0078	13.39

On the other hand, the results in Table 3 show that the pore size (ranging from 12.50 to 35.06 nm) of $_{10}$Mg–K–C are larger than that of $_{10}$Mg–C (1.65 nm) due to the oxidizing substances further etching the surface of the biochar and enlarge the pore size after the loading of K, leading to the decrease of micropore volume and the specific surface area. Similar results were also obtained in the activation processing of carbon nanotubes by KOH etching (Ji et al. 2010). The XRD patterns of $_{10}$Mg–K–C catalysts showed the $_{10}$Mg–K–C had relatively intensive diffraction peaks at 2-Theta of 36.9°, 42.9°, 62.3°, 74.7°, and 78.7°, attributed to the (111), (200), (220), (311), and (222) lattice planes of MgO crystals (Chen et al. 2020). Moreover, in contrast to $_{10}$Mg–C, $_{10}$Mg–K–C mainly contained KCl and a few K_2CO_3, $K_4H_2(CO_3)_3$ crystals. The bimetallic co-impregnation process promoted the reordering and migration of KCl, K_2CO_3, $K_4H_2(CO_3)_3$ crystalline structures (Mutreja et al. 2011). The XPS results of the $_{10}$Mg–K–C catalyst are shown in Fig. 7d–g, indicating that $_{10}$Mg–KCl–C only had a Mg–O structure (at 1303.8 eV). $MgCO_3$ (at 1305.0 eV) was also present in $_{10}$Mg–KOH–C, $_{10}$Mg–K_2CO_3–C, and $_{10}$Mg–$KHCO_3$–C with the diffraction peak areas of 27.39%, 22.09%, and 39.62%, respectively. Compared to KOH and K_2CO_3, the rapid ionization by $KHCO_3$ generated maximum

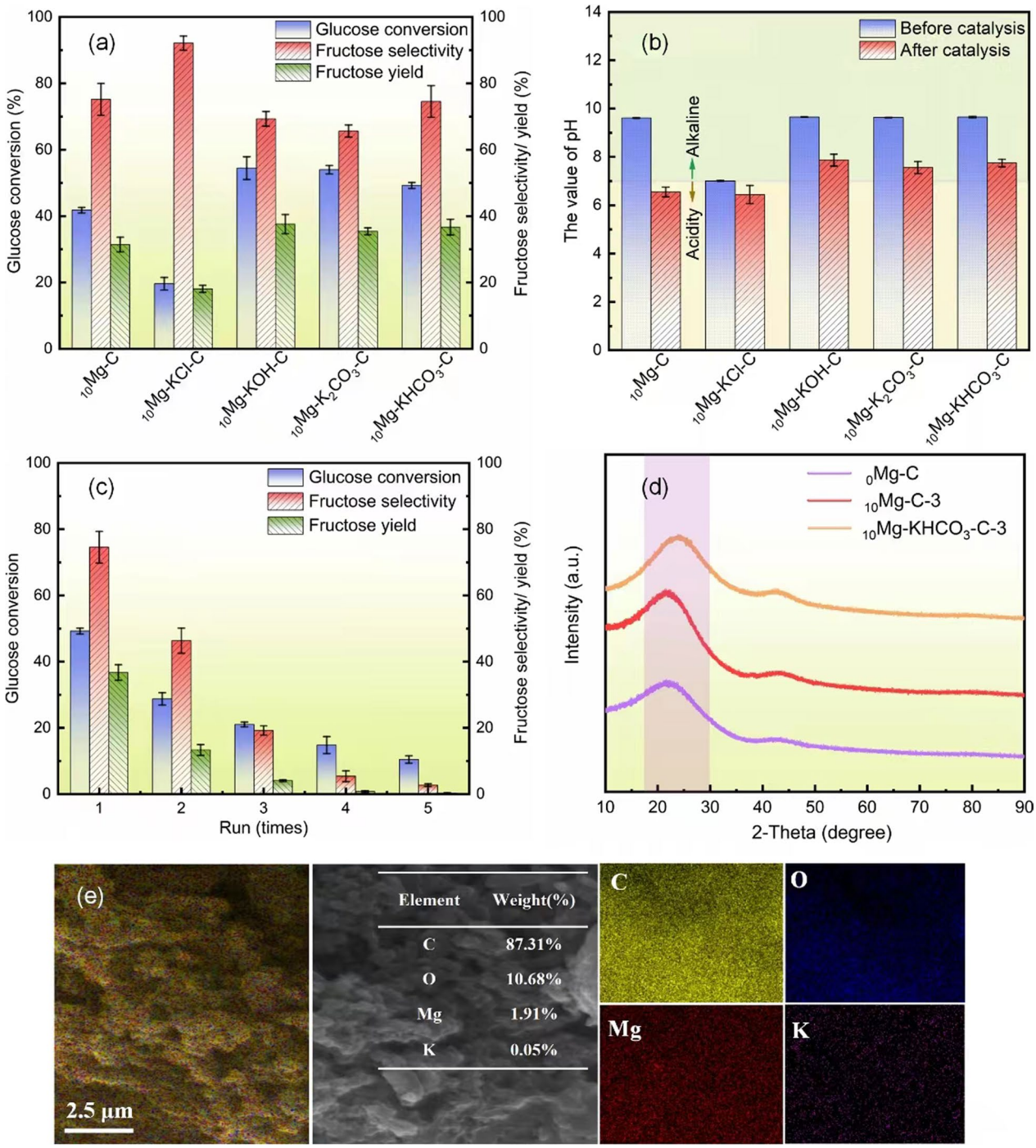

Fig. 8 Effects of different $_{10}$Mg–K–C catalysts on the **a** catalytic efficiency (conditions: 10 wt% glucose, 0.1 g catalyst, 100 °C, 30 min), **b** the pH value before and after catalysis, and the effects of $_{10}$Mg–$KHCO_3$–C catalytic cycle times on **c** the glucose isomerization catalytic efficiency, **d** the XRD spectra, and **e** the SEM–EDS images

$MgCO_3$ (39.62%) content in $_{10}$Mg–$KHCO_3$–C. The above results show that KOH, K_2CO_3, and $KHCO_3$ provided amorphous ($MgCO_3$) and crystalline (MgO, KCl, K_2CO_3, $K_4H_2(CO_3)_3$) on the $_{10}$Mg–K–C surface after co-impregnation with $MgCl_2$. Therefore, we can conclude that bimetallic co-impregnation carbonization reduced the specific surface area of the catalyst while enhancing the alkaline active sites on the

catalyst's surface by enhancing the accessibility of the active substance and glucose.

3.4 The catalytic performance and stability of $_{10}$Mg–K–C

The catalytic performance of the $_{10}$Mg–K–C catalysts under the catalytic conditions of 100 °C and 30 min is shown in Fig. 8a. Compared with $_{10}$Mg–C, the $_{10}$Mg–KOH–C, $_{10}$Mg–K_2CO_3–C, and $_{10}$Mg–$KHCO_3$–C catalysts increased the glucose conversion rate by 41.80–49.24%, 54.47%, and 53.99%, respectively, while the $_{10}$Mg–KCl–C catalyst reduced the glucose conversion rate from 41.80% to 19.64%. The obtained fructose yields catalyzed by $_{10}$Mg–K–C also presented similar results with glucose conversion rate. This is because lots of basic active sites (e.g., K_2CO_3, $K_4H_2(CO_3)_3$, and MgO) were formed in $_{10}$Mg–KOH–C, $_{10}$Mg–K_2CO_3–C, and $_{10}$Mg–$KHCO_3$–C catalysts during preparation, thus increasing catalytic efficiency and improving glucose conversion and fructose yield. The reduction in glucose conversion and fructose yield caused by $_{10}$Mg–KCl–C was due to the presence of KCl crystal in the catalyst (Fig. 8a) compared with the $_{10}$Mg–C (only MgO crystal), which decreased the alkalinity of reaction system and hindered the dissolution of OH^- ions, thus deteriorating glucose protonation (Fig. 8b). Additionally, these catalysts of $_{10}$Mg–K–C had an almost similar fructose selectivity as $_{10}$Mg–C, indicating that the common active substance MgO in all catalysts was beneficial to obtaining high fructose selectivity. These results suggest that adding crystalline and amorphous active substances by co-impregnating $MgCl_2$ with KOH, K_2CO_3, and $KHCO_3$ can preserve fructose selectivity as $_{10}$Mg–C while increasing the glucose conversion to fructose and obtaining high yield of fructose. Based on above analysis, it is concluded that the $_{10}$Mg–$KHCO_3$–C had better catalytic efficiency than other catalysts.

Glucose isomerization of catalysts is mainly driven by the ionization of the active substances caused by the OH^- ions to break glucose bonds (De Wit et al. 1979). The pH variation in the catalytic systems should be attributed to the quantity and species of active catalytic substances existing in catalysts and the leach of active substances. Simultaneously, under the same system, glucose is hydrolyzed to other by-products (furfural, 5-HMF, and organic acids), gradually decreasing the pH value of catalytic system. The presence of acidic oxidant active substances in catalytic system will attack the formed fructose to produce a cyclic fructose anion, thus decreasing the catalytic efficiency (Delidovich et al. 2014). Compared with the pH change of catalytic systems before and after catalysis (Fig. 8b), it was found that almost all catalytic systems were basic before catalysis, but after catalysis the environment became weakly acid in the catalytic systems of $_{10}$Mg–C and $_{10}$Mg–KCl–C. In combination with the catalyst results of Fig. 8a, it is concluded that basic environment caused by the catalyst both before and after catalysis such as in the $_{10}$Mg–KOH–C, $_{10}$Mg–K_2CO_3–C, and $_{10}$Mg–$KHCO_3$–C catalytic systems was beneficial to achieving high glucose conversion, fructose selectivity, and fructose yield. Different with the $_{10}$Mg–KCl–C, a relatively high fructose yield was still obtained by $_{10}$Mg–C catalysis, which should be due to the high pH value in catalytic system caused by catalyst before catalysis. Thus, a low pH caused by catalyst before catalysis would be detrimental to the basic catalytic isomerization (Brown Jr et al. 1999), and the weak basicity of the solution after catalysis can accelerate the occurrence of isomerization reactions.

The $_{10}$Mg–$KHCO_3$–C catalyst was reused, and its catalytic performance was investigated in order to evaluate its stability. The glucose conversion rate and selectivity of fructosedecreased with an increase in the reuse times (Fig. 8c). When the catalyst was used twice, the glucose conversion rate decreased from 49.24% to 29.78%, and the yield and selectivity of fructose decreased from 36.76%

Table 4 Catalytic efficiency comparison of different biochar-based metal catalysts on glucose isomerization

Catalyst	References	Catalysis conditions (solvent)	Fructose yield (%)	Glucose conversion (%)
$N_{0.5}/HC_{240}$-RO_{400}	Yang et al. (2022)	120 °C–45 min (H_2O)	31.10	32–38.00
CS-CaO-800	Shen et al. (2019)	80 °C–40 min (H_2O)	29.20	40.90
20%Al–500N_2	Yu et al. (2019)	160 °C–20 min (acetone/H_2O)	21.50	20–40.00
HC_{200}–$Al_{10\%}$–$KHCO_3$	Zhang et al. (2020a)	160 °C–20 min (H_2O)	32.60	34.10
Al/HC-300	Liu et al. (2021b)	160 °C–20 min (acetone/H_2O)	24.40	31–35.00
EG-MgO-BC-600-N_2	Chen et al. (2020)	100 °C–20 min (H_2O)	30.00	–
$_4$Mg–$_1$Al–C*		100 °C–30 min (H_2O)	22.40	31.50
Mg–Al–$KHCO_3$–C*			38.37	44.12

*The catalyst prepared from this work

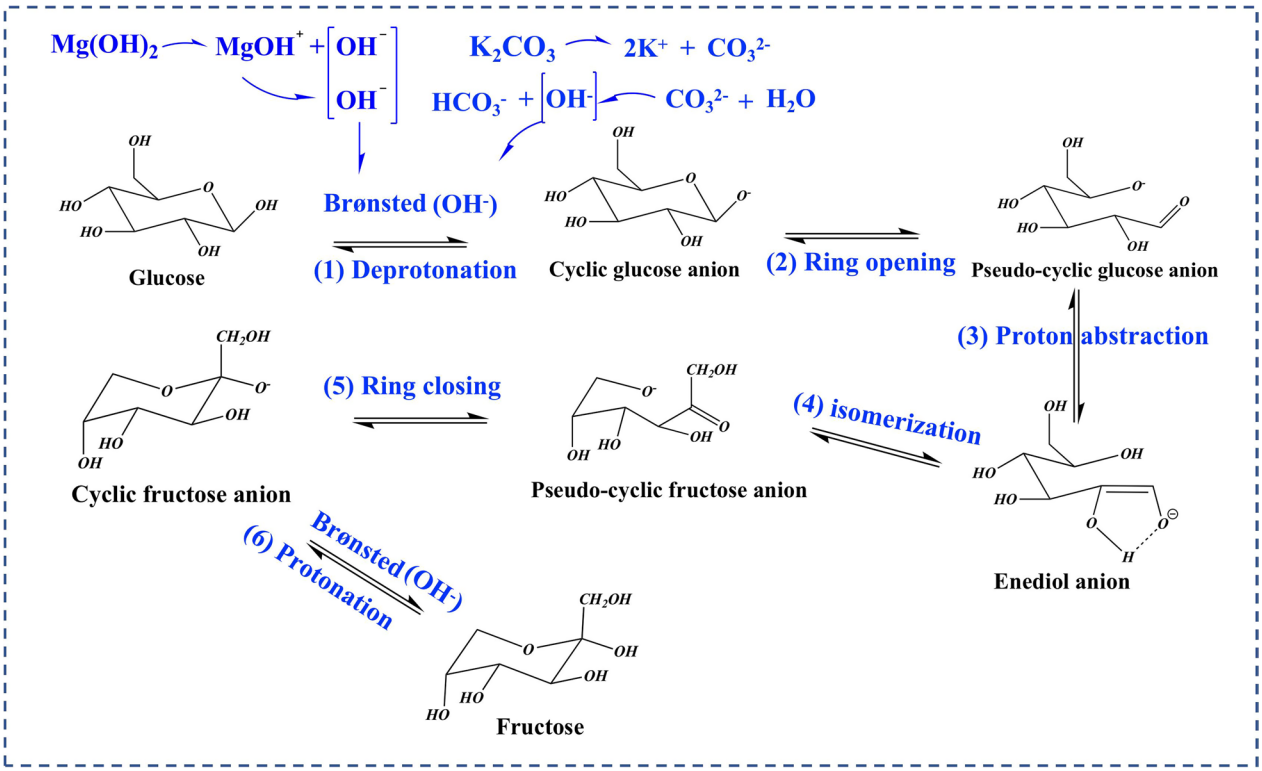

Scheme 1 Diagram of the catalytic mechanism of $_{10}$Mg–$KHCO_3$–C catalyst on glucose isomerization fructose

to 14.27% and from 74.54% to 49.38%, respectively. The Mg leaching rate of the $_{10}$Mg–K–C catalyst during the reuse process was tested in order to evaluate the stability of the catalyst (Additional file 1: Fig. S2). The results demonstrated that after the first used, the Mg leaching rate only reached 12.48%, 36.12%, 15.84%, and 16.81% in $_{10}$Mg–KCl–C, $_{10}$Mg–KOH–C, $_{10}$Mg–$KHCO_3$–C, and $_{10}$Mg–K_2CO_3–C catalyst, respectively. As the reuse time increased, the leaching rate further increased. As shown in Fig. 8d, e, the XRD analysis of the $_{10}$Mg–$KHCO_3$–C catalyst after three uses revealed the disappearance of the MgO, K_2CO_3, and $K_4H_2(CO_3)_3$ diffraction peaks, and the SEM–EDS analysis results also indicated that only part of Mg^{2+} ions (1.91%) and K^+ ions (0.05%) were remained on the surface of catalyst microspheres. Thus, the dissolution of active substances may contribute to the negative stability.

3.5 Catalytic mechanism of $_{10}$Mg–K–C

The catalytic performance of different biochar-based metal catalysts is summarized in Table 4. The 29.2–32.6% fructose yield, 71.3–93.3% fructose selectivity, and 34.1–40.9% glucose conversion were obtained using the reported biochar-based metal catalysts. In this study, the $_{10}$Mg–C and $_{10}$Mg–$KHCO_3$–C catalyst maintained the same level of used times as the existing studies (Table 4). 36.7% fructose yield, 75% fructose selectivity, and 54% glucose conversion were achieved using the $_{10}$Mg–$KHCO_3$–C catalyst, higher than most reported catalysts, particularly fructose yield and glucose conversion rate. The catalytic mechanism was discussed through the above analysis results.

$$MgO(s)_{solution} + H_2O(l) \rightarrow Mg(OH)_2(s)_{solution} \quad (1)$$

$$Mg(OH)_2(s)_{solution} \rightarrow Mg^{2+}{}_{solution} + 2OH^-{}_{solution} \quad (2)$$

$$MgO(s)_{surface} + H_2O(l) \rightarrow MgOH^+{}_{surface} + OH^-{}_{solution} \quad (3)$$

$$MgOH^+{}_{surface} + OH^-{}_{solution} \rightarrow MgOH^+ \cdot OH^-{}_{surface} \quad (4)$$

$$2KHCO_3 \xrightarrow{\Delta} K_2CO_3 + H_2O \uparrow + CO_2 \uparrow \quad (5)$$

$$K_2CO_3 + -CH_2 \xrightarrow{\Delta} K_2O + 2CO \uparrow + H_2 \uparrow \quad (6)$$

$$K_2CO_3 + 2 - CH \xrightarrow{\Delta} K_2O + 3CO \uparrow + H_2 \uparrow \quad (7)$$

$$K_2O + H_2O \xrightarrow{\Delta} 2KOH \quad (8)$$

Based on above studies, the loaded active substances and their synergism were the key factors to influence the catalytic efficiency, which also are consistent to many studies (Carraher et al. 2015; Yoo et al. 2017; Zhang et al. 2020b). As obtained from the structural characterization of $_{10}$Mg–C, the addition of $MgCl_2$ resulted in the most of the Mg^{2+} in the form of MgO on the biochar carriers surface. The catalytic results of Mg–C also confirmed the role of MgO (Yin et al. 2021). Liu and Yin et al. have reported the same conclusions, and reaction equations are shown in (1)–(4) (Liu et al. 2021a; Yin et al. 2021). But the suitable loading amount of MgO will provide better catalytic efficiency and avoid the excess MgO attack fructose. The researches from Suttibut, Drabo, and Yin et al. have demonstrated the main catalytic pathway of MgO for glucose isomerization in water is due to the dissolution of MgO transforming the hydrolyzed H_2O to OH^- ions, which attack the glucose moiety through the deprotonate reaction (Drabo et al. 2021; Suttibut et al. 2015; Yin et al. 2021) as shown in Scheme 1. Analysis of the catalytic results of $_{20}$Mg–C showed that too high Mg^{2+} loading amount (20 wt%) induced the yield of the fructose because the MgO can attack the fructose which already formed. The work from Xinhua Qi et al. has reported the same results that active sites can further attack the formed fructose (Fu et al. 2021a). Additionally, the high Mg^{2+} loading amount (20 wt%) would lead to the low specific surface area of the biochar carrier, thus reducing the transfer between the catalyst and the glucose. The amount of MgO loading will affect the catalytic efficiency and the properties of the substrate. But the XRD results also showed that the difference loading amount will not affect the crystalline structure of Mg^{2+}. Thus, we conclude that 10 wt% loading of $_{10}$Mg–C catalyst can provide the higher fructose yield (31.42%), fructose selectivity (75.17%), and glucose conversion (41.80%) at 100 °C for 30 min than $_{20}$Mg–C. De Wit et al. postulated the reaction process of glucose under the Brønsted basic condition (De Wit et al. 1979). Initially, the glucose monosaccharide is deprotonated to form a cyclic anion under Brønsted basic condition caused by active substances (reaction 1). This is followed by the transfer of a negative charge to O5 under the equilibrium between the cyclic carbonyl anion and the cyclic anion, resulting in a ring opening reaction to form pseudo-cyclic glucose anion (reaction 2). Immediately afterwards, the intramolecular proton in pseudo-cyclic glucose anion is transferred from C2 to O5, leading to proton abstraction from the pseudo-cyclic glucose anion to generate an enediol anion intermediate (reaction 3). The enediol anion acts as an important intermediate in the glucose isomerization process, which generates a pseudo-cyclic fructose anion (reaction 4). Subsequently, the double bond of the pseudo-cyclic fructose anion is broken, and a closed loop reaction occurs (reaction 5). Meanwhile, the O^- proton on the branched chain of cyclic fructose anion is further deprotonated to produce fructose due to the presence of the OH^- ions (reaction 6). Furthermore, the isomerization reaction of glucose is reversible, and the enolization rate of fructose is normally faster than that of glucose under the same reaction system. The presence of active substances in catalytic system will further attack the formed fructose to produce a cyclic fructose anion (reaction 6), and the formed enediol anion intermediate will be transformed to acidic by-products with a high selectivity due to its high activity. Therefore, reducing the production of acidic by-products and avoiding the occurrence of re-isomerization reaction are important ways to improve the yield of fructose. And tailoring the amount and type of active substances in catalyst can greatly improve glucose isomerization efficiency (Brown Jr et al. 1999). In order to further improve the isomerization efficiency of catalyst, $_{10}$Mg–$KHCO_3$–C, $_{10}$Mg–K_2CO_3–C, $_{10}$Mg–KCl–C, and $_{10}$Mg–KOH–C were prepared on the basis of $_{10}$Mg–C. Based on the catalytic effects of the $_{10}$Mg–KCl–C catalyst containing KCl and MgO crystals and the $_{10}$Mg–C catalyst containing MgO crystal, it is concluded that the synergism of KCl and MgO crystals lead to a decrease in catalytic efficiency of glucose isomerization. This is because KCl cannot provide more basic active sites for the $_{10}$Mg–KCl–C catalyst. Meanwhile, the additional KCl crystal blocks the pore size (1.61 nm, Table 3) of the biochar, thus hindering the transfer of MgO. The bimetallic co-impregnation process of $MgCl_2$ and K-containing compounds ($KHCO_3$, K_2CO_3, KOH) with biochar promotes the reordering and migration of K^+ substances (Mutreja et al. 2011), and produces same active substances such as MgO and K_2CO_3 crystalline (Fig. 7c). In the isomerization catalytic process, K_2CO_3 and MgO can produce abundant OH^- ions from H_2O to deprotonate the glucose monosaccharide to form a cyclic anion, and then the O^- proton of cyclic anion is further deprotonated to produce fructose (Mutreja et al. 2011). And the reaction equations are shown in (5)–(8) (Liu et al. 2021a). Combined with the results of catalytic isomerization (Fig. 8a), the catalytic of $_{10}$Mg–$KHCO_3$–C on glucose is mainly together determined by these active substances (MgO and K_2CO_3 crystalline). These same active substances in catalysts of $_{10}$Mg–$KHCO_3$–C, $_{10}$Mg–K_2CO_3–C, and $_{10}$Mg–KOH–C dominate the catalytic mechanism. Therefore, the catalytic mechanism of $_{10}$Mg–$KHCO_3$–C is also applicable to $_{10}$Mg–K_2CO_3–C and $_{10}$Mg–KOH–C catalyst, as shown in Scheme 1.

4 Conclusions

A highly efficient glucose isomerization catalyst, $_{10}$Mg–$KHCO_3$–C, was successfully synthesized and resulted in a 36.7% fructose yield, 74.54% fructose selectivity, and 53.99% glucose conversion at 100 °C for 30 min. Analysis of the catalytic performanceshowed that the single active substance MgO can obtain good catalytic effect on glucose isomerization, but the catalytic effect was decreased when the Mg^+ was overloaded. The synergy effects of MgO and K_2CO_3 active sites induce H_2O ionization to form considerable OH^- ions, thus easily realizing deprotonation of glucose. This work improved the efficiency of glucose isomerization to fructose and provided an efficient method for cellulose valorization.

Supplementary Information

The online version contains supplementary material available at https://doi.org/10.1007/s42773-023-00250-w.

Additional file 1: Figure S1. Mg loading contents in Mg–C catalysts. **Figure S2.** Mg leaching contents in Mg–K–C catalysts.

Acknowledgements

This work was supported by grant from the National Natural Science Foundation of China (Grant No. 22268007); Natural Science Foundation of Guangxi Province, China (Grant No. 2021GXNSFDA196006); Guangxi Science and Technology Major Pro-gram (Guike AA22117013); National Key Research and Development Program of China (Grant No. 2021YFE0114400); Innovation Project of Guangxi Graduate Education (Grant No. YCBZ2023020); and the Foundation of Guangxi Key Laboratory of Clean Pulp & Papermaking and Pollution Control, College of Light Industry and Food Engineering, Guangxi University (Grant No. 2021KF20). The authors would like to thank Professor Xueping Song and Arthur J.Ragauskas for excellent technical support and critically reviewing the manuscript. Mrs. Liu [autoclave reactor (BS-500, Shanghai LABE Instrument Co., Ltd)] was acknowledged to provide autoclave reactor. And, the authors would like to thanks "Home for researchers" for the language editing.

Author contributions

XK: conceptualization, data curation, investigation, methodology, project administration, supervision, validation, visualization, writing—original draft, writing—review & editing; ZY: methodology, validation, visualization; JP: resources, software; AJR: formal analysis, funding acquisition, writing—review & editing; JP: methodology; PZ: methodology; YY: validation; XS: methodology, project administration, supervision, validation, visualization, writing—original draft, writing—review & editing. All authors read and approved the final manuscript.

Funding

This work was sponsored by the National Natural Science Foundation of China (Grant No. 22268007); Natural Science Foundation of Guangxi Province, China (Grant No. 2021GXNSFDA196006); Guangxi Science and Technology Major Pro-gram (Guike AA22117013); National Key Research and Development Program of China (Grant No. 2021YFE0114400); Innovation Project of Guangxi Graduate Education (Grant No. YCBZ2023020); and the Foundation of Guangxi Key Laboratory of Clean Pulp & Papermaking and Pollution Control, College of Light Industry and Food Engineering, Guangxi University (Grant No. 2021KF20). AJR efforts were supported University of Tennessee, Knoxville.

Availability of data and materials

The datasets generated during and/or analyzed during the current study are available from the corresponding author on reasonable request.

Declarations

Competing interests

The authors declare that they have no known competing financial interests or personal relationships that could have appeared to influence the work reported in this paper.

Author details

[1]Guangxi Key Laboratory of Clean Pulp & Papermaking and Pollution Control, College of Light Industry and Food Engineering, Guangxi University, Nanning 530004, People's Republic of China. [2]Department of Chemical and Biomolecular Engineering, University of Tennessee, Knoxville, TN, USA. [3]Oak Ridge National Laboratory, Biosciences Division, Joint Institute for Biological Sciences, Oak Ridge, TN, USA. [4]Center for Renewable Carbon, Department of Forestry, Wildlife and Fisheries, The University of Tennessee, Knoxville, TN 37996, USA. [5]School of Electrical and Power Engineering, China University of Mining and Technology, Xuzhou 221116, People's Republic of China. [6]China CAMC Engineering CO., LTD., SINOMACH Plaza, No. 3, Danling Street, Beijing 100080, People's Republic of China.

Received: 28 February 2023 Revised: 22 July 2023 Accepted: 24 July 2023
Published online: 08 September 2023

References

Ahmad J, Cordioli E, Patuzzi F, Prando D, Castaldi MJ, Baratieri M (2016) Possible utilization pathways of char from biomass thermochemical conversion: char as a catalytic filtering medium for tar cracking. In: 24th international European biomass conference on setting the course for a biobased economy, Jun 06–09, Amsterdam. pp 475–479

Ahmad J, Vakalis S, Patuzzi F, Baratieri M (2020) Effect of process conditions on the surface properties of biomass chars produced by means of pyrolysis and CO_2 gasification. Energy Environ 32(8):1378–1396. https://doi.org/10.1177/0958305x20948237

Brown GE Jr, Henrich VE, Casey WH, Clark DL, Eggleston C, Felmy A, Goodman DW, Grätzel M, Maciel G, McCarthy MI, Nealson KH, Sverjensky DA, Toney MF, Zachara JM (1999) Metal oxide surfaces and their interactions with aqueous solutions and microbial organisms. Chem Rev 99:77–174. https://doi.org/10.1021/CR980011Z

Carraher JM, Fleitman CN, Tessonnier J-P (2015) Kinetic and mechanistic study of glucose isomerization using homogeneous organic Brønsted base catalysts in water. ACS Catal 5(6):3162–3173. https://doi.org/10.1021/acscatal.5b00316

Chai X, He H, Fan H, Kang X, Song X (2019) A hydrothermal-carbonization process for simultaneously production of sugars, graphene quantum dots, and porous carbon from sugarcane bagasse. Bioresour Technol 282:142–147. https://doi.org/10.1016/j.biortech.2019.02.126

Chen SS, Cao Y, Tsang DCW, Tessonnier J-P, Shang J, Hou D, Shen Z, Zhang S, Ok YS, Wu KCW (2020) Effective dispersion of MgO nanostructure on biochar support as a basic catalyst for glucose isomerization. ACS Sustain Chem Eng 8(18):6990–7001. https://doi.org/10.1021/acssuschemeng.0c00278

De Wit G, Kieboom APG, van Bekkum KH (1979) Enolisation and isomerisation of monosaccharides in aqueous, alkaline solution. Carbohydr Res 74(1):157–175. https://doi.org/10.1016/j.carres.2004.06.004

Delidovich IV, Simonov AN, Taran OP, Parmon VN (2014) Catalytic formation of monosaccharides: from the formose reaction towards selective synthesis. ChemSusChem 7(7):1833–1846. https://doi.org/10.1002/cssc.201400040

Deng Y, Zhang T, Clark J, Aminabhavi T, Kruse A, Tsang DCW, Sharma BK, Zhang F, Ren H (2020) Mechanisms and modelling of phosphorus solid–liquid transformation during the hydrothermal processing of swine manure. Green Chem 22(17):5628–5638. https://doi.org/10.1039/d0gc01281e

Ding Z, Zhang L, Mo H, Chen Y, Hu X (2021) Microwave-assisted catalytic hydrothermal carbonization of *Laminaria japonica* for hydrochars catalyzed and activated by potassium compounds. Bioresour Technol 341:125835. https://doi.org/10.1016/j.biortech.2021.125835

Drabo P, Fischer M, Toussaint V, Flecken F, Palkovits R, Delidovich I (2021) What are the catalytically active species for aqueous-phase isomerization of

D-glucose into D-fructose in the presence of alkaline earth metal (hydr) oxides? J Catal 402:315–324. https://doi.org/10.1016/j.jcat.2021.08.036
Falco C, Baccile N, Titirici M-M (2011) Morphological and structural differences between glucose, cellulose and lignocellulosic biomass derived hydrothermal carbons. Green Chem 13(11):3273–3281. https://doi.org/10.1039/c1gc15742f
Fu J, Shen F, Liu X, Qi X (2021a) Synthesis of MgO-doped ordered mesoporous carbons by Mg^{2+}-tannin coordination for efficient isomerization of glucose to fructose. Green Energy Environ 406:126748. https://doi.org/10.1016/j.gee.2021.11.010
Fu Q, Yang S, Ning P, Miao R, He L, Guan Q (2021b) Construction of dot-matrix Cu_0–Cu_1Ni_3 alloy nano-dispersions on the surface of porous N-auto-doped biochar for selective hydrogenation of furfural. ChemCatChem 13(19):4164–4181. https://doi.org/10.1002/cctc.202100882
Ji L, Shao Y, Xu Z, Zheng S, Zhu D (2010) Adsorption of monoaromatic compounds and pharmaceutical antibiotics on carbon nanotubes activated by KOH etching. Environ Sci Technol 44(16):6429–36. https://doi.org/10.1021/es1014828
Kang X, Wang YY, Wang S, Song X (2021) Xylan and xylose decomposition during hot water pre-extraction: a pH-regulated hydrolysis. Carbohydr Polym 255:117391. https://doi.org/10.1016/j.carbpol.2020.117391
Kang X, Peng J, Ragauskas AJ, Ren X, Si C, Wang S, Song X (2022) Competitive effects of glucan's main hydrolysates on biochar formation: a combined experiment and density functional theory analysis. Bioresour Technol 359:127427. https://doi.org/10.1016/j.biortech.2022.127427
Kim D, Yoshikawa K, Park K (2015) Characteristics of biochar obtained by hydrothermal carbonization of cellulose for renewable energy. Energies 8(12):14040–14048. https://doi.org/10.3390/en81212412
Kim M, Jee S-C, Sung J-S, Kadam AA (2020) Supermagnetic sugarcane bagasse hydrochar for enhanced osteoconduction in human adipose tissue-derived mesenchymal stem cells. Nanomaterials 10(9):1793. https://doi.org/10.3390/nano10091793
Kuichuan Sheng SZ, Liu J, Shuang E, Jin C, Xu Z, Zhang X (2019) Hydrothermal carbonization of cellulose and xylan into hydrochars and application on glucose isomerization. J Clean Prod 237:117831. https://doi.org/10.1016/j.jclepro.2019.117831
Lazzarini A, Piovano A, Pellegrini R, Leofanti G, Agostini G, Rudić S, Chierotti MR, Gobetto R, Battiato A, Spoto G, Zecchina A, Lamberti C, Groppo E (2016) A comprehensive approach to investigate the structural and surface properties of activated carbons and related Pd-based catalysts. Catal Sci Technol 6(13):4910–4922. https://doi.org/10.1039/c6cy00159a
Li B, Li L-W, Dong Y-N, Zhang Q, Weng W-Z, Wan H-L (2018) Glucose isomerization into fructose catalyzed by MgO/NaY catalyst. Chin J Chem Phys 31(2):203–210. https://doi.org/10.1063/1674-0068/31/cjcp1709183
Liu J, Yang M, Gong C, Zhang S, Sheng K, Zhang X (2021a) Insights into the glucose isomerization mechanism of Al-hydrochar catalyst probed by Al-oxide species transformation. J Environ Chem Eng 9(6):106721. https://doi.org/10.1016/j.jece.2021.106721
Liu J, Zhang X, Yang L, Danhassan UA, Zhang S, Yang M, Sheng K, Zhang X (2021b) Glucose isomerization catalyzed by swollen cellulose derived aluminum-hydrochar. Sci Total Environ 777:146037. https://doi.org/10.1016/j.scitotenv.2021.146037
Liu X, Fu J, Tang Y, Smith RL Jr, Qi X (2021c) Mg-coordinated self-assembly of MgO-doped ordered mesoporous carbons for selective recovery of phosphorus from aqueous solutions. Chem Eng J 406:126748. https://doi.org/10.1016/j.cej.2020.126748
Marianou AA, Michailof CM, Pineda A, Iliopoulou EF, Triantafyllidis KS, Lappas AA (2016) Glucose to fructose isomerization in aqueous media over homogeneous and heterogeneous catalysts. ChemCatChem 8(6):1100–1110. https://doi.org/10.1002/cctc.201501203
Marianou AA, Michailof CM, Ipsakis DK, Karakoulia SA, Kalogiannis KG, Yiannoulakis H, Triantafyllidis KS, Lappas AA (2018) Isomerization of glucose into fructose over natural and synthetic MgO catalysts. ACS Sustain Chem Eng 6(12):16459–16470. https://doi.org/10.1021/acssuschemeng.8b03570
Mutreja V, Singh S, Ali A (2011) Biodiesel from mutton fat using KOH impregnated MgO as heterogeneous catalysts. Renew Energy 36(8):2253–2258. https://doi.org/10.1016/j.renene.2011.01.019
Rabee AIM, Le SD, Nishimura S (2020) MgO–ZrO(2) mixed oxides as effective and reusable base catalysts for glucose isomerization into fructose in aqueous media. Chem Asian J 15(2):294–300. https://doi.org/10.1002/asia.201901534
Shen F, Fu J, Zhang X, Qi X (2019) Crab shell-derived lotus rootlike porous carbon for high efficiency isomerization of glucose to fructose under mild conditions. ACS Sustain Chem Eng 7(4):4466–4472. https://doi.org/10.1021/acssuschemeng.8b06512
Song Z, Lian F, Yu Z, Zhu L, Xing B, Qiu W (2014) Synthesis and characterization of a novel MnOx-loaded biochar and its adsorption properties for Cu^{2+} in aqueous solution. Chem Eng J 242:36–42. https://doi.org/10.1016/j.cej.2013.12.061
Suttibut P, Suriye K, Kunjara Na Ayudhya S, Praserthdam P, Panpranot J (2015) Effect of N_2 pretreatment on the basicity, structural change, and isomerization activity of MgO and $MgO/Mg(OH)_2$ catalysts. Asia Pac J Chem Eng 10(2):248–258. https://doi.org/10.1002/apj.1869
Yang Y, Hu C-W, Abu-Omar MM (2012) Conversion of carbohydrates and lignocellulosic biomass into 5-hydroxymethylfurfural using $AlCl_3{\cdot}6H_2O$ catalyst in a biphasic solvent system. Green Chem 14(2):509–513. https://doi.org/10.1039/c1gc15972k
Yang L, Shuang E, Liu J, Sheng K, Zhang X (2022) Endogenous calcium enriched hydrochar catalyst derived from water hyacinth for glucose isomerization. Sci Total Environ 807(Pt 2):150660. https://doi.org/10.1016/j.scitotenv.2021.150660
Yin G, Tao L, Chen X, Bolan NS, Sarkar B, Lin Q, Wang H (2021) Quantitative analysis on the mechanism of Cd(2+) removal by $MgCl_2$-modified biochar in aqueous solutions. J Hazard Mater 420:126487. https://doi.org/10.1016/j.jhazmat.2021.126487
Yoo CG, Li N, Swannell M, Pan X (2017) Isomerization of glucose to fructose catalyzed by lithium bromide in water. Green Chem 19(18):4402–4411. https://doi.org/10.1039/c7gc02145c
Yu IKM, Xiong X, Tsang DCW, Wang L, Hunt AJ, Song H, Shang J, Ok YS, Poon CS (2019) Aluminium-biochar composites as sustainable heterogeneous catalysts for glucose isomerisation in a biorefinery. Green Chem 21(6):1267–1281. https://doi.org/10.1039/c8gc02466a
Zhang S, Sheng K, Liang Y, Liu J, Shuang E, Zhang X (2020a) Green synthesis of aluminum-hydrochar for the selective isomerization of glucose to fructose. Sci Total Environ 727:138743. https://doi.org/10.1016/j.scitotenv.2020.138743
Zhang S, Wang J, Zhu S, Liu X, Xiong Y, Zhang H (2020b) Effects of $MgCl_2$ and $Mg(NO_3)_2$ loading on catalytic pyrolysis of sawdust for bio-oil and MgO-impregnated biochar production. J Anal Appl Pyrol 152:104962. https://doi.org/10.1016/j.jaap.2020.104962

Submit your manuscript to a SpringerOpen journal and benefit from:

- ► Convenient online submission
- ► Rigorous peer review
- ► Open access: articles freely available online
- ► High visibility within the field
- ► Retaining the copyright to your article

Submit your next manuscript at ► springeropen.com